

System Identification Modeling for Flight Control Design

Christina M. Ivler

Aerospace Engineer

Mark B. Tischler

Flight Control Group Lead

Aeroflightdynamics Directorate (AMRDEC)

US Army Research, Development, and Engineering Command
Ames Research Center, Moffett Field, CA

Abstract

Flight control analyses require accurate models of the bare airframe and its associated uncertainties, as well as the integrated system (block diagrams) across the frequency range of interest. Frequency domain system identification methods have proven to efficiently fulfill these requirements in recent rotorcraft flight control applications. This paper presents integrated system identification methods for flight control modeling for flight test examples of the Fire Scout MQ-8B, S-76, and ARH-70A. The paper also looks toward how system identification could be used in new modeling challenges such as the Joint Heavy Lift rotorcraft as well as small unique unmanned configurations.

Nomenclature

a_x, a_y, a_z	accelerometer components in body-axis	β_o	rotor coning angle
a_{x_m}, a_{y_m}	accelerations as measured at the sensor, not at the center of gravity	β_{ls}, β_{lc}	rotor lateral and longitudinal flapping angles
p, q, r	angular rates	$\delta_{ail}, \delta_{flp}, \delta_{rud}$	deflections of aileron, flaperon and rudder
T	engine torque	$\delta_{lon}, \delta_{lat}, \delta_{ped}, \delta_{col}$	longitudinal, lateral, pedal, and collective pilot control input
u, v, w	body-axis velocities	ε_r	random error
u_m, v_m	velocities as measured at the sensor, not at the center of gravity	ζ, ω	damping and natural frequency of a second order system
u	vector of controls in state-space model	η_{CT}	coefficient of thrust ‘fictitious’ state
M, F, G, H_0, H_1	state-space model terms	$\eta_{XC'}$	delayed collective input for engine dynamics
x	vector of states in state-space model	μ_{wb-p}	derivative relating asymmetric wing bending to roll rate
x_e	engine delay state, used for padé approximation		

$\mu_{wb-ail} \delta_{ail}$	derivative relating asymmetric wing bending to aileron input
ϕ, θ, ψ	Euler angles
Φ_{pl}	bending mode displacement coefficient
σ	standard deviation
τ_f	flapping time constant
ν	inflow
ν_ζ	regressive lag frequency in the rotating frame
ω_c	cross-over frequency
Ω_R	rotor speed with respect to the fuselage

Introduction

Most flight control design methodologies require a linear model that accurately represents the aircraft that is to be controlled. For example, classical feedback design (root locus), quantitative feedback theory, LQR, eigenstructure-assignment, and linear dynamic inversion techniques are all examples of control techniques that use linear state-space models or transfer functions. Additionally, linear models are also used in direct parametric optimization techniques such as CONDUIT[®] (Ref. 1). When a prototype aircraft is available, frequency domain system identification can be used to develop state-space models directly from flight data (Ref. 2). This method has been proven to be highly accurate and efficient, and also has the benefit of providing uncertainty parameters.

Frequency domain system identification has been used to develop linear vehicle models for many recent rotorcraft applications such as the CH-47 (Ref. 3), ARH (Ref. 4), S-76 (Ref. 5), UH-60MU (Ref. 6), and Fire Scout (Ref. 7). In most cases, these system identification models were used for flight control design even when physics based models were available. The reasons for this include:

1. A model based on flight data will better match the dynamics of the actual vehicle.
2. System identification is more time efficient than attempting to correct the physics based model to better match flight data.
3. The identified model provides additional physical insight to the control designer (which in many cases is later used to correct the physics based model).
4. Uncertainty data are readily available for the identified model.

For most of these rotorcraft applications, the flight control engineers were also responsible for performing the system identification. This generally provided the flight control group with more control over the degrees

of freedom in the model, greater understanding of the model fidelity, and ultimately resulted in a better integration of modeling and flight control development.

It is well known that “the quality and accuracy of the mathematical models describing the basic flight vehicle (and its subsystems) used for the flight control law design have a tremendous impact on the quality of the control laws and the achievable control bandwidth” (Ref. 8). Therefore, it is important to look ahead to flight control design during the linear model determination process, and be careful to take into account degrees of freedom that are important in the frequency range of interest for flight control design. It is also equally important during flight control design to look back to the linear model development process and perform uncertainty analysis to determine the effect of modeling uncertainties on the control system. This is due to the fact that “uncertainties in the models can lead to sub-optimal controller operations, reduced flight performance, and very often result in additional costs” (Ref. 8). The best practice, therefore, is to accomplish both modeling and control law development in an integrated way. The system identification tool CIFER[®] (Ref. 2) and the control design tool CONDUIT[®] (Ref. 1) can be used to implement this methodology of integrated modeling, control design, and uncertainty analysis.

Several recent rotorcraft flight test applications in modeling and flight control design will serve as case studies in this paper. These example cases will demonstrate the added value provided through integrated system identification modeling, flight control design, and uncertainty analysis. This paper also looks towards how this methodology can be used in future rotorcraft challenges.

Frequency Domain System Identification Methods

The system identification methodology has four main steps: frequency response identification, state-space model fitting to the MIMO frequency response database, model structure determination and time domain verification. The methodology is well suited to rotorcraft identification due to its insensitivity to uncorrelated output noise (which produces a bias in time-domain methods), and its ability to identify unstable dynamics (which is also difficult in the time domain due to divergence). The steps are discussed below, and with greater detail in Ref. 2.

1. Frequency response identification from flight data (Chirp-Z transform)

First, a Chirp-Z transform with overlapping windows is used to initially transform time-domain frequency sweep data to the frequency-domain. Then, multi-input conditioning is used to condition out the effect of any off-axis inputs that occurred during the frequency

sweep. Finally, the frequency range of accuracy is improved by combining a weighted average of multiple windows, in a method known as Composite Windowing. The result is a high quality MIMO frequency response database.

2. State space model identification

A state-space model structure is chosen by the user, based on analysis of the frequency responses. Then, the freed state-space model parameters are optimized to match the frequency responses identified from flight data. A coherence weighted cost function (J) is used to quantify the match between flight data and the state-space model. The uniqueness and validity of each parameter is tested by calculating the Insensitivities (I) and Cramer-Rao Bounds (CR).

3. Model structure determination

Parameters that have undesirably large insensitivities and/or Cramer-Rao bounds are systematically removed from the model structure. The model is re-converged after each parameter is removed. This ensures that all parameters are sensitive to the cost function and that there are no correlated parameters in the model.

4. Time domain verification

Once a model that matches the flight data in the frequency domain has been determined, the model is verified in the time domain using data that was not previously used in the identification process. Doublets in each axis are usually used for verification. The state-space model is driven with flight data, and the outputs of the model are evaluated against the real flight data. A cost function is again used to measure the match between the model and the flight data.

These steps are implemented by the CIFER[®] software in the analyses presented in this paper.

Flight Control Requirements

The flight control requirements drive the type and fidelity of the model used. Key modeling requirements for rotorcraft flight control include:

1. Model must be a very accurate match of the flight data.

There are two types of model fidelity that must be considered for helicopter flight control design (Ref. 9):

a) Functional fidelity - the level of fidelity required to predict flying qualities parameters.

b) Physical fidelity - the ability of the model to represent the underlying physics.

2. Model must be valid over the frequency range of interest.

This is generally from 1/3 to 3 times the broken-loop cross-over frequency of the system, because modes in

this frequency range contribute substantially to the closed loop response (Ref. 10). However, the model may need to extend even further to accurately identify the gain margin, which occurs at the ω_{180} frequency of the broken loop response (Ref. 2).

3. Uncertainty models are needed for assessment of system robustness.

A best practice is to define a set of model uncertainties that can be used as design tolerances (Ref. 8).

4. Broken and closed-loop block diagrams should be validated against flight data to ensure that all flight control, actuator, mixer, and other subsystem models are accurately integrated into the block diagram.

“The accurate predication of broken-loop and closed-loop frequency responses establishes a critical anchor point for the control system model” (Ref. 2).

System identification helps with meeting the above requirements:

The model must be a very accurate match of the flight data – System identification ensures that the model matches the flight data, since it is identified and verified against flight. The match of the model to the flight data is characterized by a cost function in the system identification method which helps facilitate the engineer in determining whether the match to flight data is acceptable. The use of a model structure that incorporates physical parameters ensures that the identification values are physically meaningful. The hybrid model (Ref. 2), which combines rotor states for the mid-to-high frequency range and quasi-steady derivatives for low frequency, is an example of a model structure that incorporates physically meaningful parameters.

The model must be valid over the frequency range of interest – The coherence function provides information about the frequency range of accuracy of a non-parametric (frequency-response) model. If the frequency response is accurate over the frequency range of interest, then an accurate parametric model should also be able to be identified over that same range. If the model does not fit flight data over that frequency range, additional degrees of freedom can be modeled to simulate the dynamics seen at those frequencies.

Uncertainty Models are needed – Non-parametric models (i.e. frequency responses) have a random error associated with them that can be estimated. This gives an indication of the amount of error in the frequency response at any given frequency. These error bounds can be used in the analysis if the frequency response is used in the flight control design. Theoretical uncertainty known as the Cramer-Rao bounds can be calculated for the identified state-space model parameters. The use of the Cramer-Rao bound as an uncertainty parameter is very common and can be integrated into the flight

control analysis.

Aircraft subsystems must be validated – The use of frequency sweeps in flight can be used to identify broken and closed loop responses of the aircraft with the control system. If the open loop and closed loop flight frequency responses match those from the block diagram (which includes the aircraft linear model and subsystem models), then the block diagram subsystems can be assumed to be validated. If the broken and closed loop responses do not match, identification of individual subsystems on the aircraft can be carried out until the source of the mismatch is determined.

Case Studies for Integrated System Identification and Flight Control

A series of case studies are shown to exemplify how system identification was used to meet the flight control

requirements given in the previous section for recent rotorcraft flight control development applications. Three different case studies are given; MQ-8B Fire Scout UAV, S-76D, and the ARH-70A. For these case studies, creative modeling solutions were found in order to meet the flight control requirements. This trio of case studies demonstrates the flexibility of the method and the variety of the ways in which it has been successfully used.

Fire Scout

The Fire Scout is being developed as a ship-based VTOL UAV for the U.S. NAVY. The MQ-8B, which is the current version of the Fire Scout, has an upgraded transmission, four rotor blades (as opposed to three on the earlier configuration, RQ-8A), and minor modifications to the airframe as compared to the RQ-8A. The MQ-8B Fire Scout is depicted in Fig. 1.



Figure 1. MQ-8B first hover (reprinted from Ref. 7).

Frequency domain system identified models were exclusively used for the Fire Scout flight control design. A physics model was not available, so the identified linear models at various speed conditions across the envelope were “stitched” together with trim data and velocity based interpolation in order to provide for a continuous full-envelope simulation model. The Fire Scout program had many unique requirements that required careful consideration during model identification and flight control design/analysis. These challenges included:

1. To determine whether a 6 DOF model was sufficient for flight control design.
2. The need for reasonably accurate rotor rpm and torque modeling, since torque feedback was to be used in the control system.
3. A requirement to perform uncertainty analysis of the final flight control design.

The following sections of the paper will provide highlights of the model identification, flight control design, and uncertainty analysis for the Fire Scout UAV. The hover flight condition will be shown throughout as an example.

Hover Model Structure

The first task in the modeling of the Fire Scout was determining the model structure. This required the engineers to discern whether a quasi-steady 6 DOF model would be sufficient to meet the fidelity requirements for flight control design at hover. For many rotorcraft, higher order rotor-states are needed in order to accurately model the aircraft over the frequency range of interest. In order to determine whether a quasi-steady model was adequate, the intended bandwidth of the control system as well as the rotor characteristics were considered.

The first consideration made in determining the validity of the use of a 6 DOF model was the frequency range of interest. According to flight control requirement #2, in the previous section of this paper:

$$\frac{1}{3}\omega_c \leq \text{Freq Range of Interest} \leq 3\omega_c \quad (1)$$

The required cross-over frequency ω_c for roll and pitch axis was planned to be around 3-4 rad/s. Therefore it was important to have a good model between approximately 1 rad/s to 12 rad/s.

For a rotor system that is moderately stiff, such as the Fire Scout rotor, a quasi-steady (6 DOF) model was found to be valid up to 10-12 rad/s. A time delay was

also included to represent the effect of unmodeled rotor dynamics on the phase. This was possible because the rotor flapping and fuselage roll response modes are decoupled in a low or moderately stiff rotor. Engine and torque states were also included in the state-space structure to meet the requirement to obtain an accurate model of the torque. The final model structure was:

$$M\dot{x} = Fx + Gu(t - \tau) \quad (2)$$

$$y = H_0x + H_1\dot{x} \quad (3)$$

$$x = [u \ v \ w \ p \ q \ r \ \phi \ \theta \ \Omega_R \ \Omega \ \dot{\Omega} \ T]^T \quad (4)$$

$$y = [\dot{u} \ \dot{v} \ \dot{w} \ a_x \ a_y \ a_z \ p \ q \ r \ \Omega_R \ T]^T \quad (5)$$

$$u = [\delta_{lon} \ \delta_{lat} \ \delta_{ped} \ \delta_{col}]^T \quad (6)$$

Note that $\Omega = \Omega_R - r$, where Ω_R is the rotor response with respect to the fuselage (Ω is defined in the opposite sign of fuselage yaw rate, r).

A model of the torque response was needed to simulate the torque response and to design a torque feedback controller. Thus, the additional states $[\Omega_R \ \Omega \ \dot{\Omega} \ T]^T$ were included for the engine and torque dynamics. A simple Taylor-series expansion was used to model the torque:

$$\dot{T} = T_t T + T_\Omega \Omega + T_{\delta_{col}} \delta_{col} + T_{\delta_{ped}} \delta_{ped} \quad (7)$$

The rotor speed was modeled as a second order system with a washout:

$$\frac{\Omega}{\delta_{col}} = \frac{sK_{\delta_{col}}}{(s^2 + 2\zeta\omega_s + \omega^2)(s + a)} \quad (8)$$

Additionally, the rotor-rpm dynamics were coupled to the roll and yaw rate responses to collective in order to model the phase delay that is associated with the engine response. This was done by including L_Ω and N_Ω as effective control derivatives in the equations of motion instead of using $L_{\delta_{col}}$ and $N_{\delta_{col}}$.

Example Hover Results for Fire Scout Model

The accuracy of the identified state-space models for Fire Scout was quantified by the identification cost functions, as well as visual overlays of time and frequency domain responses with flight data. The

responses were well predicted with the presented model structure over the frequency range of interest (1-12 rad/s) as indicated by the average cost function:

$$J_{avg} = 79.4 \quad (9)$$

An average cost function below 100 is considered a very good model. As an example of the model accuracy, Fig. 2 shows the on-axis longitudinal responses for hover. The cost functions for these two individual responses were:

$$J_{q/\delta_{lon}} = 60.2 \quad (10)$$

$$J_{\dot{u}/\delta_{lon}} = 45.9 \quad (11)$$

The cost functions for these model fits were well within the desired values (<150-200) for an individual frequency response. A cost of 50 (or less) is considered a nearly perfect model. The primary responses for the other axes exhibited similar accuracy, and the coupling responses also maintained adequate fidelity (Ref. 7). This indicated that the model fidelity was good enough for flight control design.

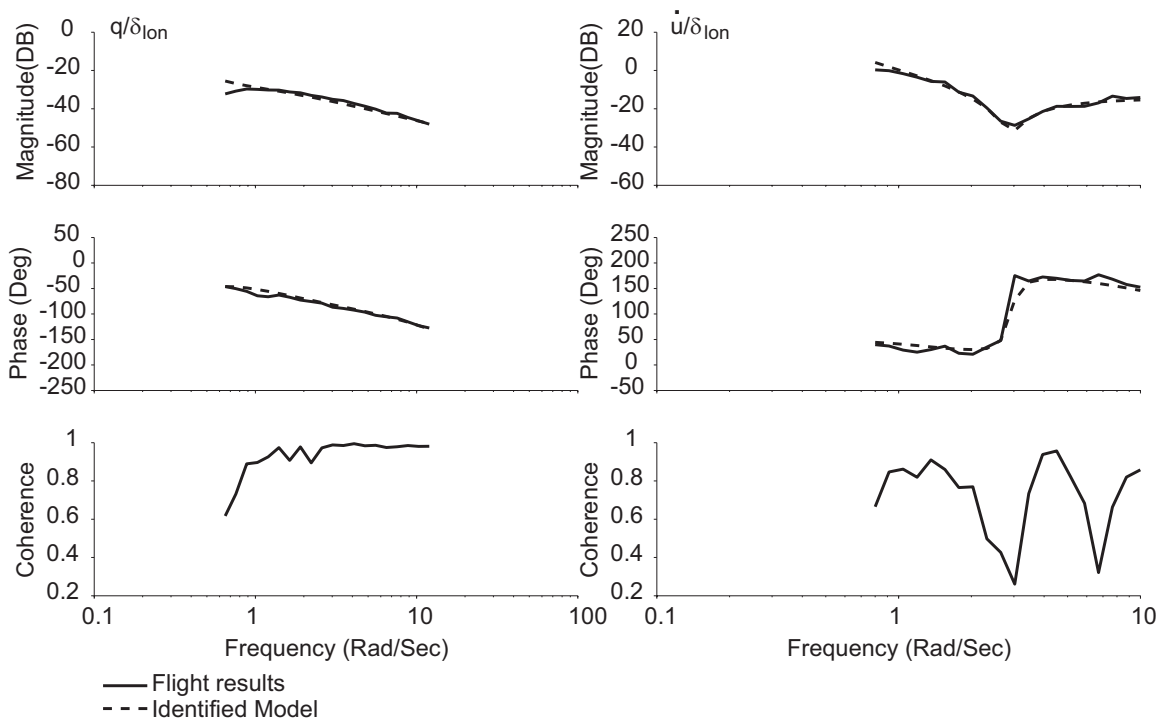


Figure 2. On-axis longitudinal responses comparison to flight data for MQ-8B at hover.

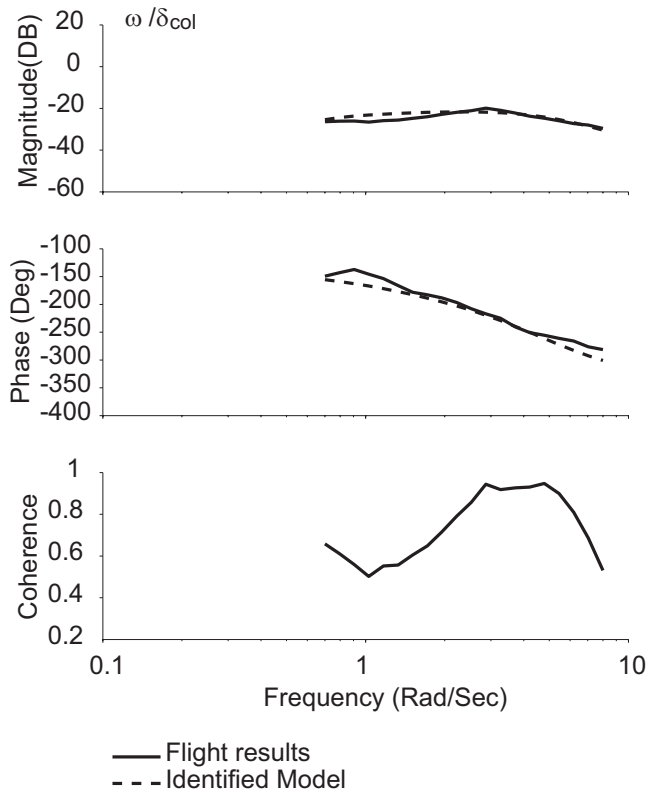


Figure 3. RPM comparison to flight data for MQ-8B at hover.

The simple engine and torque modeling method was effective over a wide frequency range, as shown in Fig. 3 and by the values of the cost functions:

$$J_{T/\delta_{col}} = 58.5 \quad (12)$$

$$J_{\Omega/\delta_{col}} = 59.8 \quad (13)$$

This indicated that the engine modeling method was accurate and could be used for simulation and feedback control design.

As an example of the time domain accuracy of the model, the results are shown for the longitudinal and

heave axes in Fig. 4 and Fig. 5. The pitch and roll responses to the longitudinal input were very well predicted in the time domain. The mismatch in the yaw rate coupling response comes from poor data in the associated frequency response r/δ_{lon} , which made it difficult to accurately identify these coupling derivatives. Even so, the magnitude of the coupling is correct, although slightly out of phase. The lateral and directional axes show similar accuracy but are not depicted here for brevity. For full results, see Ref. 7, as this paper shows example results that can be considered representative.

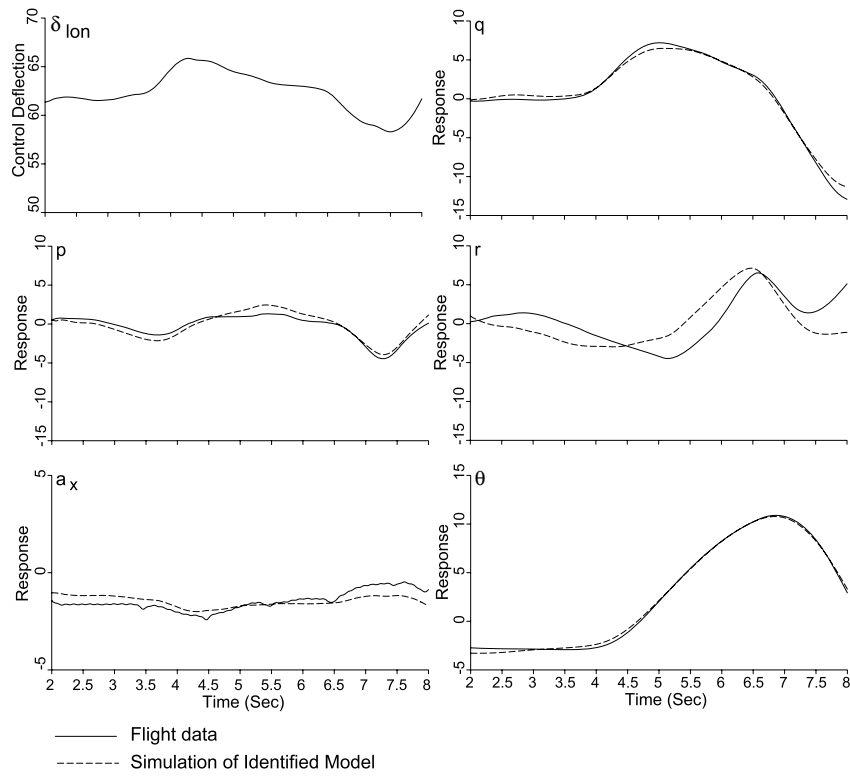


Figure 4. Longitudinal verification results for MQ-8B at hover.

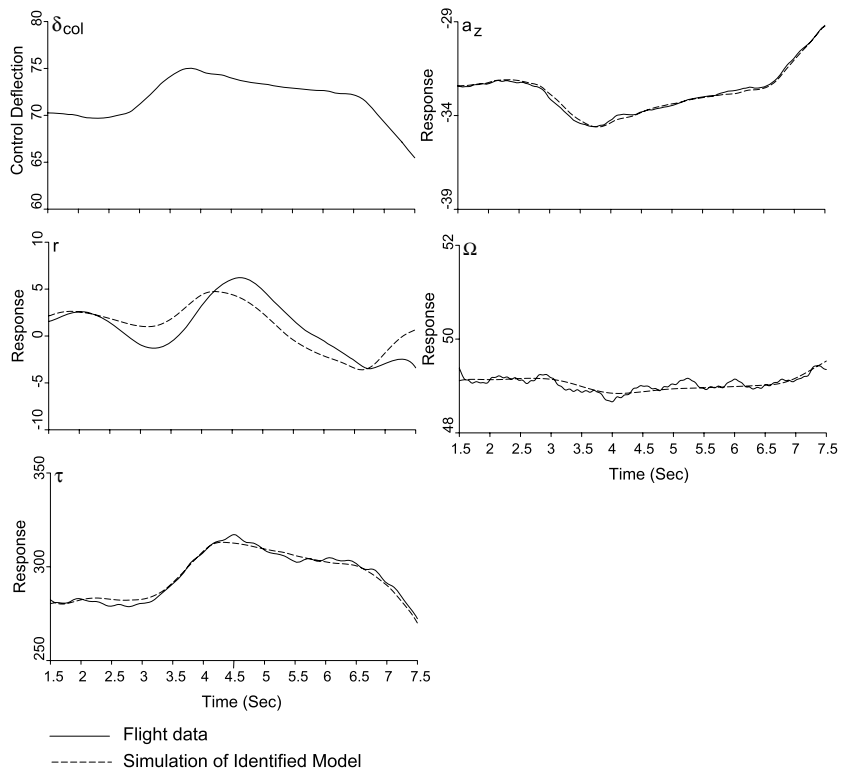


Figure 5. Heave verification results for MQ-8B at hover.

Inner Loop Control Law Design

After the model was identified and verified to be accurate, the next step in the process was to perform control design. The inner loop architecture was a basic attitude command attitude hold PID-type control system for pitch, roll, and yaw. The vertical axis was a rate command system implemented as a PI controller on the vertical velocity, with a torque feedback loop. Two methods of control law optimization were used – the CONDUIT[®] software developed by AFDD and an NGC implemented genetic algorithm. Both methods utilized the identified linear models. The results of the

optimizations were compared to provide confidence in the control law design results. Table 1 shows the specifications that were considered key in the optimizations. The results of the two optimizations turned out very similar, as shown in Table 2, and thus provided confidence in the flight control design.

Once the control law design was optimized and cross-checked between the two design methodologies, the next step was to test the performance of the system under uncertain conditions.

Table 1. Key MQ-8B Specifications.

Specification	Description
Stability Margins	Ensures that stability margins are met for the nominal control system design.
ADS-33 Bandwidth	Ensures that the UAV meets piloted bandwidth requirements since it is a full sized rotorcraft, and good flying qualities are desired even though it is not piloted.
Disturbance Rejection Bandwidth	Ensures that the system will reject disturbances. This is very important for ship operations of a UAV.
Damping Ratio	Ensures that lightly damped oscillations are not allowed. This is important for precision operations.
Cross-over Frequency	Ensures that the cross-over frequency of the system is minimized (CONDUIT [®]) to ensure actuators are not overused. For Genetic algorithms, user checks that cross-over frequency is reasonable.

Table 2. Comparison of CONDUIT[®] and genetic algorithm designs for MQ-8B.

	Pitch G.M. (dB)	Pitch P.M. (deg)	Roll G.M. (dB)	Roll P.M. (deg)	Yaw G.M. (dB)	Yaw P.M. (deg)	Collective G.M. (dB)	Collective P.M. (deg)
CONDUIT [®]	8.5	46.1	8.32	48.7	16.7	45	7.1	45
Genetic	9.3	40.5	6.4	42	8.1	49.8	22.7	44.9
	Pitch Crossover (rad/s)	Roll Crossover (rad/s)	Yaw Crossover (rad/s)	Collective Crossover (rad/s)	Pitch D.R.B. (rad/s)	Roll D.R.B. (rad/s)	Yaw D.R.B. (rad/s)	Collective D.R.B. (rad/s)
CONDUIT [®]	3.92	4.18	2.82	2.14	0.96	1.4	1.1942	0.98
Genetic	3.39	4.68	4.98	2.2	.949	1.75	1.21	1.209

G.M. = gain margin, P.M. = phase margin, D.R.B. = disturbance rejection bandwidth

Uncertainty Analysis

For Fire Scout, uncertainties in the identified stability and control derivatives were considered. For this parametric uncertainty analysis, the Cramer-Rao bounds of the individually identified parameters from the Fire Scout state-space model were considered. Cramer-Rao

bounds represent the theoretical accuracy of the identified derivatives in the state-space model (Ref. 2). The Cramer-Rao bounds provided by CIFER[®] are scaled to represent the expected standard deviation in the identified parameters:

$$(CR_i)_{cifer} \approx \sigma_i \quad (14)$$

Thus, there was a direct measure of the uncertainty for each identified parameter in the state-space model. The effect of these uncertainties on the stability of the system was analyzed for the hover control laws. In order to take into account a 99.7% confidence interval, each derivative that has an associated Cramer-Rao bound was randomly perturbed by $\pm 3\sigma$. The random term only determines whether the derivative should be perturbed positively or negatively, not the absolute size of the perturbation, which was fixed at $|3\sigma|$. Using this method, there are a finite number of possible perturbed models - $2^{(\#free_parameters)}$. However, with 32 free parameters in the hover model, there were 4.29E9 possible perturbed models. By randomly perturbing all derivatives at one time and then looking at the effect on the stability, one can determine how severely the

combinations of uncertainty affect the system and whether more robustness needs to be built into the control laws.

CONDUIT[®] has access to the CIFER[®] database, and has a built in robustness tool that perturbs the model based on its Cramer-Rao bounds. The final results are shown in the handling qualities window of Fig. 6 for 250 random perturbations of $\pm 3\sigma$. All axes remain stable, even with such a large perturbation of the stability and control derivatives. The perturbations most affect the vertical loop which is shown in the bottom right of Fig. 6. The phase margin lost 20 degrees, and the gain margin was reduced by 7dB relative to the nominal design in the vertical axis. The stability margins are still within 50% of the original 6dB and 45 degree boundaries, as required by AS94900 for an uncertainty (or “sensitivity”) analysis of the critical stability derivatives (Ref 11).

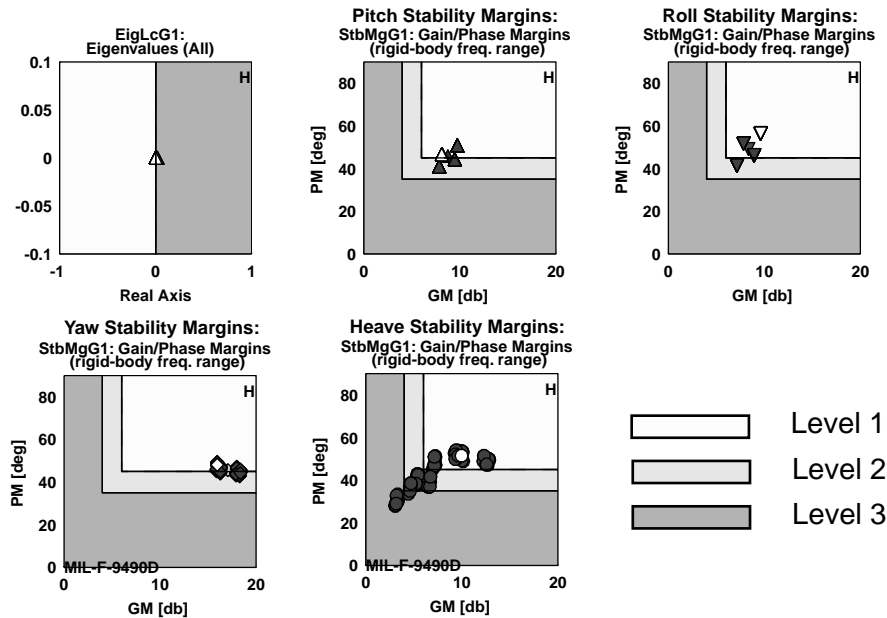


Figure 6. Parametric uncertainty analysis for MQ-8B at hover.

Lessons Learned on Fire Scout

System identification was utilized in the Fire Scout model identification process, flight control design, and uncertainty analysis. The system identification models produced accurate predictions of the aircraft dynamics for flight control analysis, which were then utilized in the flight control design. These models were easily implemented into the linear flight control law design simulations, and the engineers had the advantage of

understanding the model states and accuracy in the design process since they had themselves produced the models. Finally, the uncertainty analysis showed that the control system design was robust to the uncertainties that were identified with the model. All these components worked together to provide confidence in the final design.

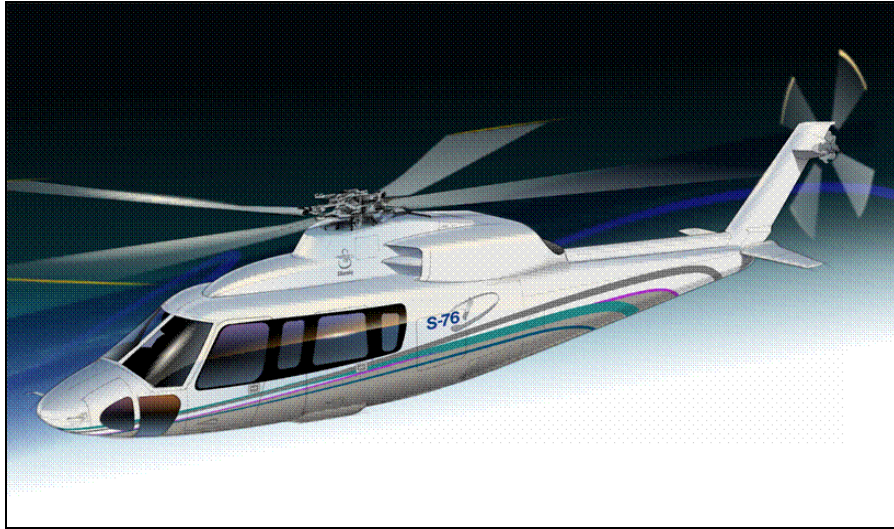


Figure 7. S-76D.

S-76

The S-76 is a light twin-engine, four bladed helicopter that has been operating since the 1970s. The newest upgrade, the S-76D, will feature a Thales automatic flight control system (AFCS). The S-76D is pictured in Fig. 7.

In order to develop an automatic flight control system, the S-76 team was required to provide accurate models of the aircraft to the Thales AFCS developers. Because the S-76D was not ready for flight the S-76C, which is a similar design, was used for the initial system identification of the helicopter. This model would be used for initial AFCS design, and later updated versions of the models would be created after first flight. Thus, the key concerns for the S-76C team involved providing the best model possible for AFCS design. The following challenges related to the flight control requirements were important:

1. The model had to be very accurate over a wide frequency range to ensure accurate flight control stability analysis and handling qualities prediction.
2. The model had to be physically meaningful, as it was also used to update the nonlinear simulation model.

The modeling for the S-76 will be discussed in the following sections in order to show how the flight control challenges were met through the use of the system identification technique. The hover model will be discussed as an example of the methods used in the modeling process.

Model Structure for the S-76 at hover

The hover model was identified using piloted frequency sweeps of the S-76C helicopter. Frequency response identification was completed from these data sets. The state-space model structure was selected based on an inspection of the identified frequency responses. A wide frequency range of accuracy was needed because the model was used to check the non-linear simulation which included high frequency modes. Therefore, the frequency range of interest was chosen as 0.5-20 rad/s in this case. The shape of the frequency responses over this frequency range indicated that higher-order dynamics including coupled flap/fuselage dynamics, lead-lag dynamics, engine dynamics, and inflow-coning dynamics should be included in the S-76 hover model. The higher-order dynamics were included as necessary by implementing the hybrid model structure (Ref. 2). The hybrid model structure combines higher frequency explicit rotor dynamics with low frequency dynamics that are modeled in a quasi-steady way.

$$M\dot{x} = Fx + Gu \quad (15)$$

$$y = H_0x + H_1\dot{x} \quad (16)$$

The state, input and output vectors for the hybrid model identification were:

$$x = [u \quad v \quad w \quad p \quad q \quad r \quad \phi \quad \theta \quad \beta_{1s} \quad \beta_{1c} \quad u_m \quad v_m \quad v \quad \dot{\beta}_0 \quad \beta_0 \quad \eta_{CT} \quad x_e \quad \eta_{XC'}]^T \quad (17)$$

$$u = [\delta_{lon} \quad \delta_{lat} \quad \delta_{ped} \quad \delta_{col}]^T \quad (18)$$

$$y = [\dot{u}_m \quad \dot{v}_m \quad \dot{w} \quad p \quad q \quad r \quad a_{x_m} \quad a_{y_m} \quad a_z \quad (a_{y_m})_2]^T \quad (19)$$

In the following section, examples comparing the higher order and quasi-steady models are shown to explain why the more complex model structures were needed. For the quasi-steady model only the fuselage states were included:

$$x = [u \quad v \quad w \quad p \quad q \quad r \quad \phi \quad \theta]^T \quad (20)$$

The use of the higher order model was a key factor in obtaining a valid model over a wide frequency range.

Flap/Fuselage Dynamics

The S-76 helicopter exhibits moderate blade flap stiffness, which indicates that the on-axis responses

(q/δ_{lon} and p/δ_{lat}) were well modeled by a 6 DOF approximation for frequencies up to 8-10 rad/s. In order to extend the model further across the frequency range of interest beyond 10 rad/s, additional degrees of freedom were needed. Furthermore, a quasi-steady model did not accurately capture the phase characteristic for the off-axis responses p/δ_{lon} and q/δ_{lat} . A model structure that explicitly models the rotor flapping dynamics better predicted these off-axis responses, which is consistent with results shown in Ref. 2. Figure 8 illustrates this point with a comparison of these two models for the off-axis response p/δ_{lon} . The figure indicates that the coupling response was much better represented by the model that included flapping dynamics, as seen by the closer match to flight magnitude and phase. This is important because it is desirable to minimize coupling responses of a closed-loop aircraft to improve handling qualities, which requires a good model of the coupling responses.

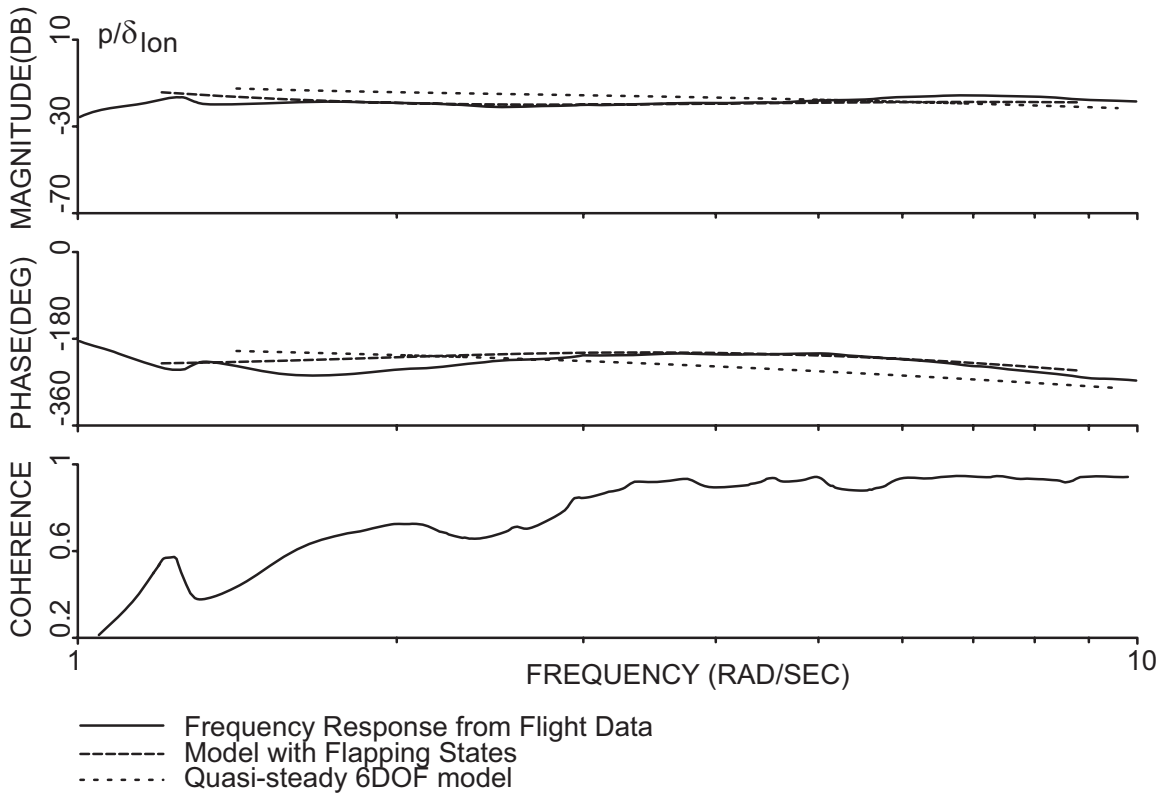


Figure 8. Off axis roll rate response from longitudinal stick for S-76 at hover.

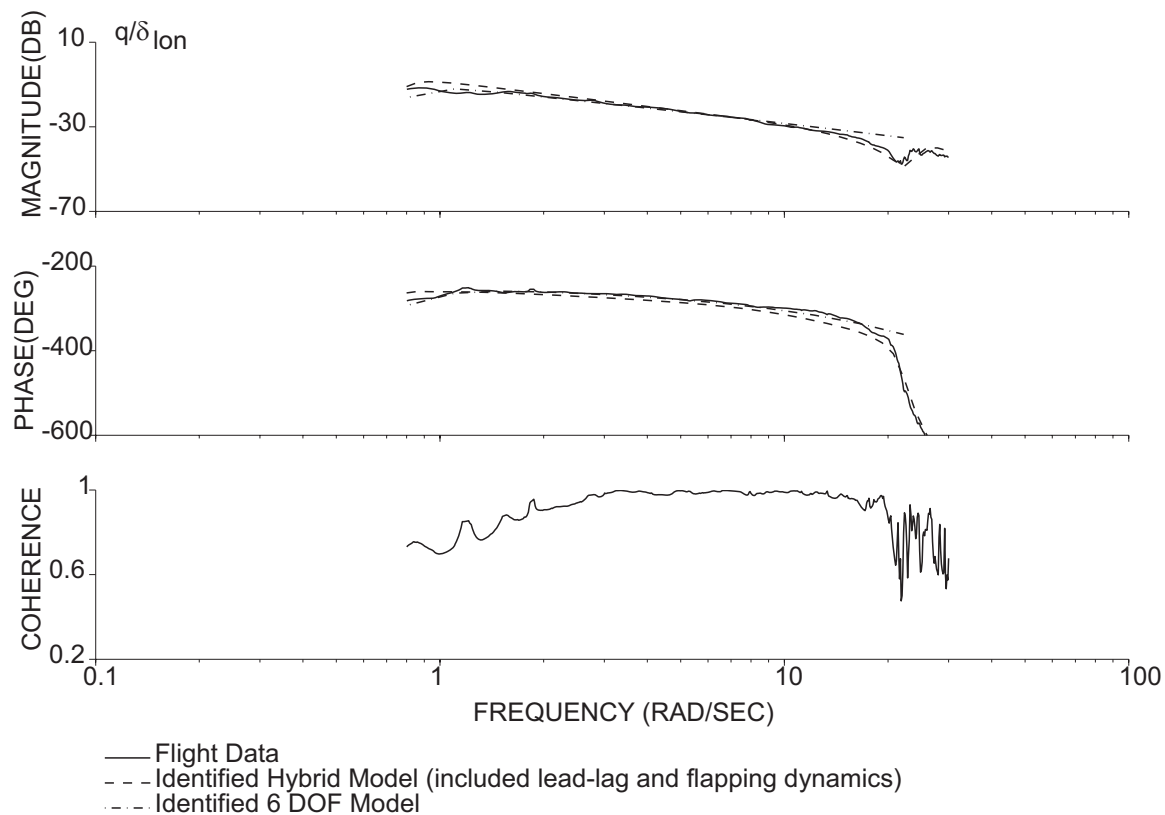


Figure 9. Pitch rate response from longitudinal stick for S-76 at hover.

Lead-Lag Dynamics

The effect of the lead-lag dynamics can be clearly seen in the on-axis pitch rate frequency response q/δ_{lon} of Fig. 9 between 20-30 rad/s. The regressive lag mode (or lead-lag dynamics) looks like a notch in the magnitude response, accompanied by a large phase shift at roughly 24 rad/s. It was clear that in order to extend the model accuracy beyond 20 rad/s, a higher order model must be included to capture these dynamics. The magnitude and phase responses were also somewhat affected by the

lead-lag mode between 15 - 20 rad/s. Since the mode was near the frequency range of interest and lightly damped, it was important to include it in a model that was intended for flight control purposes. The combination of the flapping dynamics and lead-lag mode gave a very wide frequency range of accuracy, from about 0.8 - 30 rad/s, as shown in Fig. 9. A comparison with a quasi-steady 6DOF model is given, which is only accurate to approximately 12 rad/s, as expected.

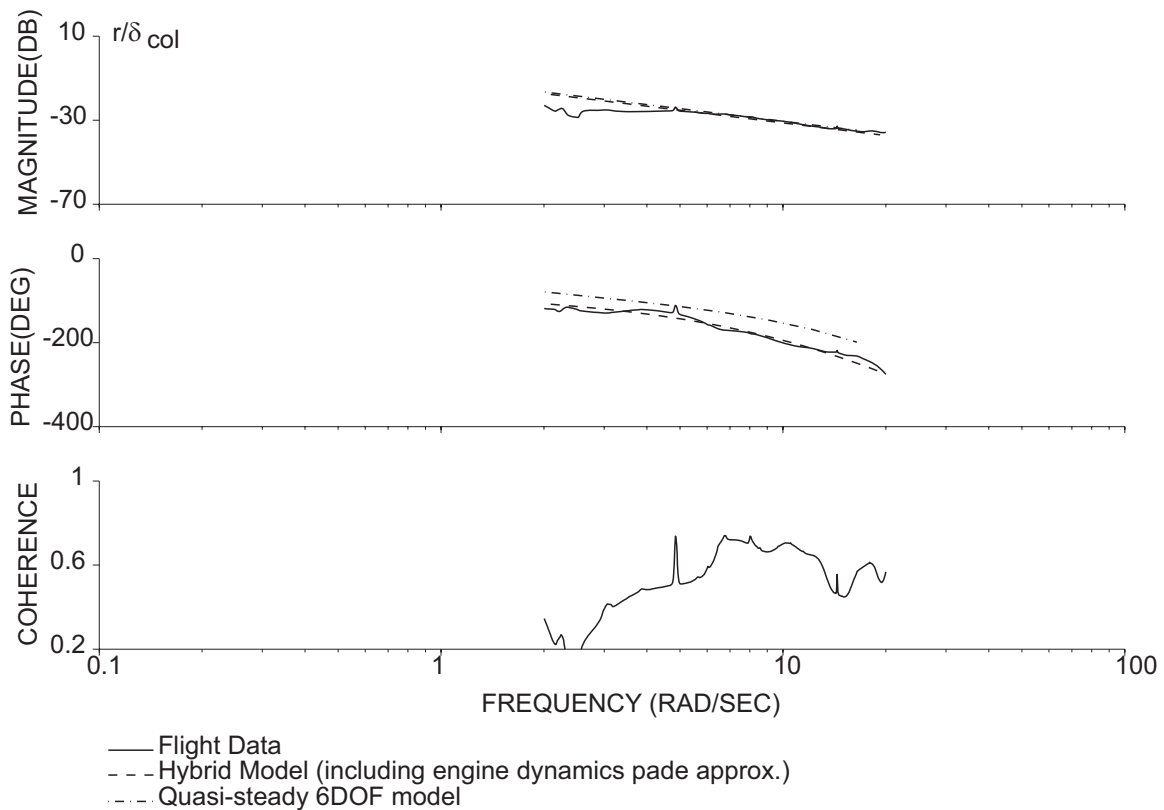


Figure 10. Yaw rate response from collective input for S-76 at hover.

Engine Dynamics

The phase curve for yaw rate to collective response r/δ_{col} of a helicopter rolls off very quickly at high frequencies. This is well known as a lag effect associated with engine dynamics. These dynamics can be modeled as a time delay on the r/δ_{col} pairing, or using simple engine equations as shown in the Fire Scout case study. For the S-76, rpm and torque states were not needed for flight control, so the time delay

method was used because it is simpler to implement. A padé approximation was included in the state-space model structure to produce the lag effect. Figure 10 shows a much improved phase response as compared to a model which does not include the engine lag. This proved to be an important modification to the model because it provided better prediction of an important coupling response that would be considered in the flight control analysis.

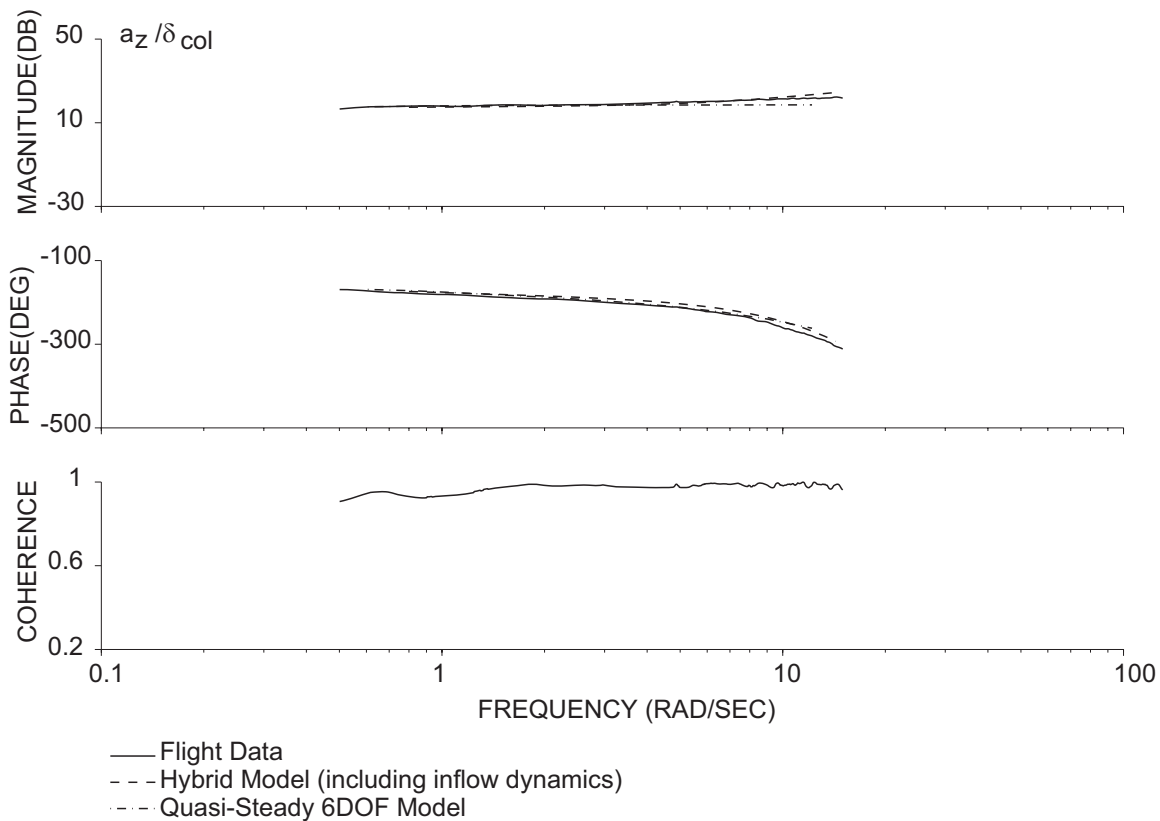


Figure 11. Vertical acceleration response from collective input, for S-76 at hover.

Coning-Inflow Dynamics

Figure 11 shows the response of vertical acceleration (a_z) to collective input for the S-76 at hover. The rising magnitude response above about 2 rad/s is the result of the coning-inflow dynamics (Ref. 2). This rise in a_z magnitude cannot be represented within a quasi-steady model structure because it creates a flat magnitude response as shown in Fig. 11. Considering that a vertical controller cross-over frequency is typically around 1-2 rad/s, it was important to include inflow dynamics to extend the frequency range of accuracy beyond 2 rad/s to provide accurate predictions of gain margin.

The use of the hybrid model to characterize certain important dynamics that cannot be captured by a quasi-steady 6 DOF model was successful in providing

functional fidelity (the match of the model to the flight data).

Time domain verification

In order to ensure that the hybrid model had good predictive accuracy in the time domain, verification was performed. The data used were doublet records, which were not previously used in the system identification process. The model provided a very good match to the flight data in the time domain as shown by the longitudinal axes examples given in Fig. 12. The other axes had similar accuracy.

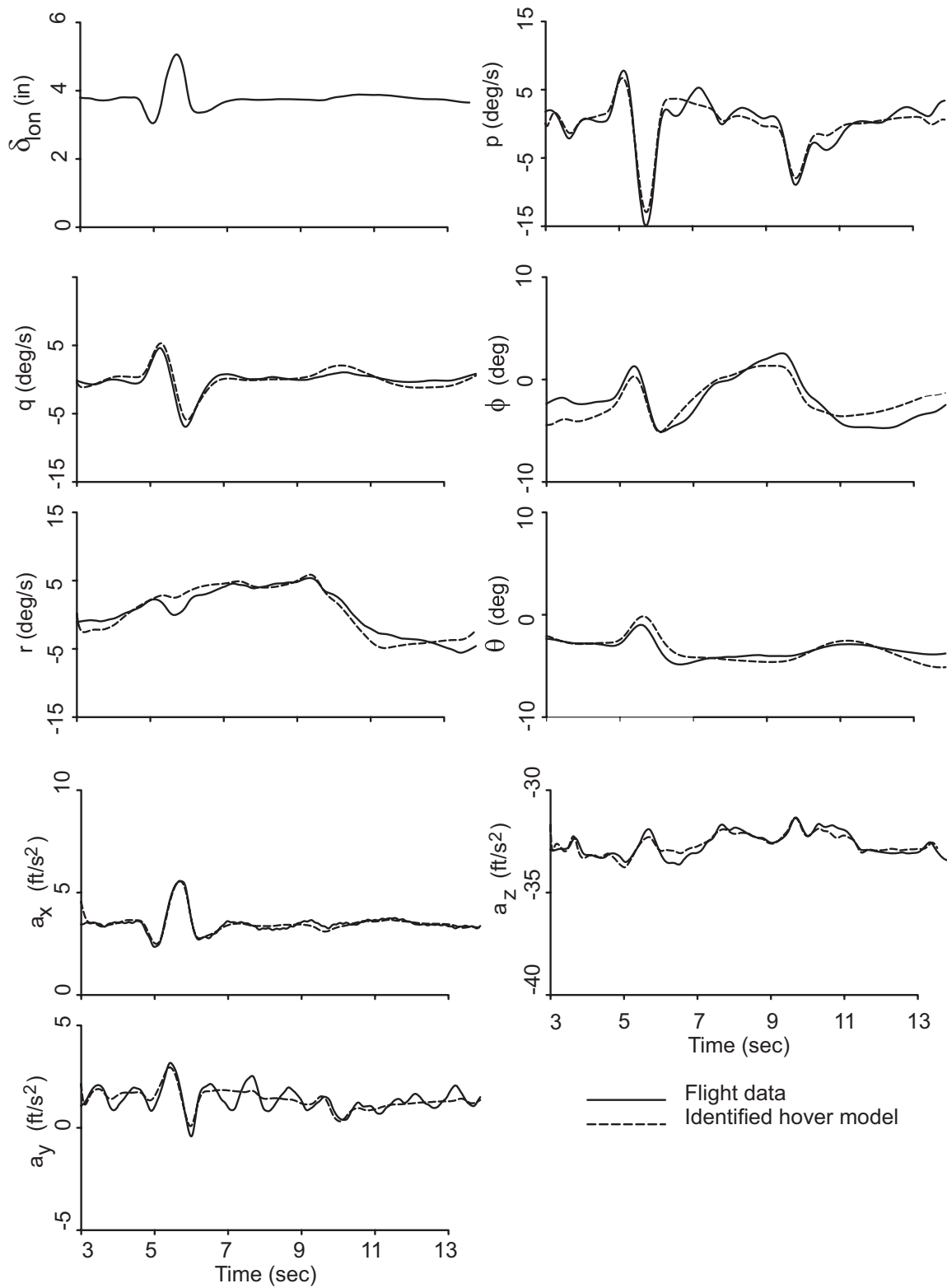


Figure 12. Longitudinal verification for S-76 at hover.

Ensuring physical fidelity of the model

Once the time domain verification was performed, it was important to analyze the S-76 model to ensure that it was physically meaningful. These checks were performed in order to meet the requirement that the model could be used to gain physical insight. The structure used on the S-76, a hybrid model, contains physically meaningful parameters since it was derived from the physics that govern the dynamics of a helicopter. For the S-76, some of these identified physical parameters were compared to theory - the flapping constant τ_f , the linear acceleration terms due to flapping $X_{\beta_{1c}}$ and $Y_{\beta_{1s}}$, and the rotating lag frequency, ν_ζ .

The flapping constant was an identified parameter. Its value was compared to the theoretical calculation (Ref. 2):

$$(\tau_f)_{theory} = \left[\frac{\gamma^* \Omega}{16} \left(1 - \frac{8e}{3R} \right) \right]^{-1} \quad (21)$$

where γ^* is the reduced Lock number

Using the equation above, the identified flap constant was shown to be consistent with theory:

$$(\tau_f)_{theory} = 0.09057 \quad (22)$$

$$(\tau_f)_{ID} = 0.09118 \quad (23)$$

Other rotor parameters that were freed in the identification were the flapping spring force terms $X_{\beta_{1c}}$ and $-Y_{\beta_{1s}}$. The theoretical value of these terms is the gravity constant (32.17 ft/s²). The identified value was close to gravity at $X_{\beta_{1c}} = -Y_{\beta_{1s}} = 30.28$. These parameters were reasonably consistent with theory considering that the small offset was likely due to uncertainty in the exact location of the vertical center-of-gravity.

The regressive lead-lag mode (in the fixed-frame) was identified with light damping ($\zeta_{llr} = 0.121$) and with a natural frequency of 25.5 rad/s (ω_{llr}). The regressive lag frequency was expressed in the rotating frame (ν_ζ) by shifting the imaginary part of the fixed frame mode by the rotor rotational speed (Ω). Then, the normalized identified lead-lag frequency was:

$$\nu_\zeta = \sqrt{\frac{(\Omega - \omega_{dllr})^2 + \sigma_{llr}^2}{\Omega^2}} = 0.241 \quad (24)$$

The theoretical value was:

$$(\nu_\zeta)_{theoretical} = \sqrt{\frac{3}{2} \left(\frac{e}{1-e} \right)} = 0.240 \quad (25)$$

The excellent agreement between the theoretical and identified values for the rotating lag frequency showed that the lead-lag model was physically meaningful and accurate.

Lessons Learned for S-76

The use of inspection of the frequency responses to determine the model structure was helpful in ensuring that the model was accurate over the frequency range of interest. This process was more time efficient than identifying a quasi-steady model at first, only to discover that it was not as accurate as desired. The accurate time and frequency domain matches of the model and flight data, as well as the close consistency of the physical parameters of the model to theory provided confidence in the final model. Because of the high accuracy of the model, the model was used to help tune the nonlinear simulation to better match the flight data. Overall, system identification provided the S-76 team with better models of the aircraft for use in simulation and for analysis of the performance of the AFCS design. More detailed results for the S-76 model identification at hover, as well as at 120 knots, can be seen in Ref. 5.



Figure 13. ARH-70A.

ARH

The Armed Reconnaissance Helicopter, ARH-70A, is being developed by Bell Helicopter to replace the OH-58. The ARH-70A is depicted in Fig. 13.

In order to meet the desire to achieve Level 1 handling qualities; the AFCS was designed to meet ADS-33E-PRF requirements. Flight identified models were developed and used in the AFCS design. The flight control requirements that were addressed through system identification included:

1. Determination and validation of accurate models for flight control design.
2. Validation of the control law block diagrams.

System identification played a key role in preparing for the flight control design of the ARH-70A. Models were identified from flight data at the following flight conditions: hover, level flight at maximum rate of climb airspeed, and level flight at 90% maximum speed with continuous power. The hover model identification and control block diagram validation will be given as examples of how system identification was used to meet ARH-70A flight control design requirements.

Model Identification at Hover

The ARH frequency sweep flight testing data was used to identify frequency-responses of the aircraft. The next step was to determine if a 6 DOF model structure was sufficient. Similarly to the Fire Scout, it was determined that since the rotor stiffness was moderate, and only moderate control cross-over frequencies were to be used, that the quasi-steady 6 DOF model was sufficient. Therefore the model structure takes the following form:

$$M\dot{x} = Fx + Gu \quad (26)$$

$$y = H_0x + H_1\dot{x} \quad (27)$$

$$x = [u \ v \ w \ p \ q \ r \ \phi \ \theta] \quad (28)$$

These models produced a match to the flight data over the frequency range of interest, which was from about 1-12 rad/s (cross-over between 3-4 rad/s). This can be seen in the comparison of the model and flight data shown in Fig. 14 for the longitudinal axis. The other axes showed similar model fidelity. Figure 15 indicates that the model was able to accurately predict the response of the aircraft in the time domain as well.

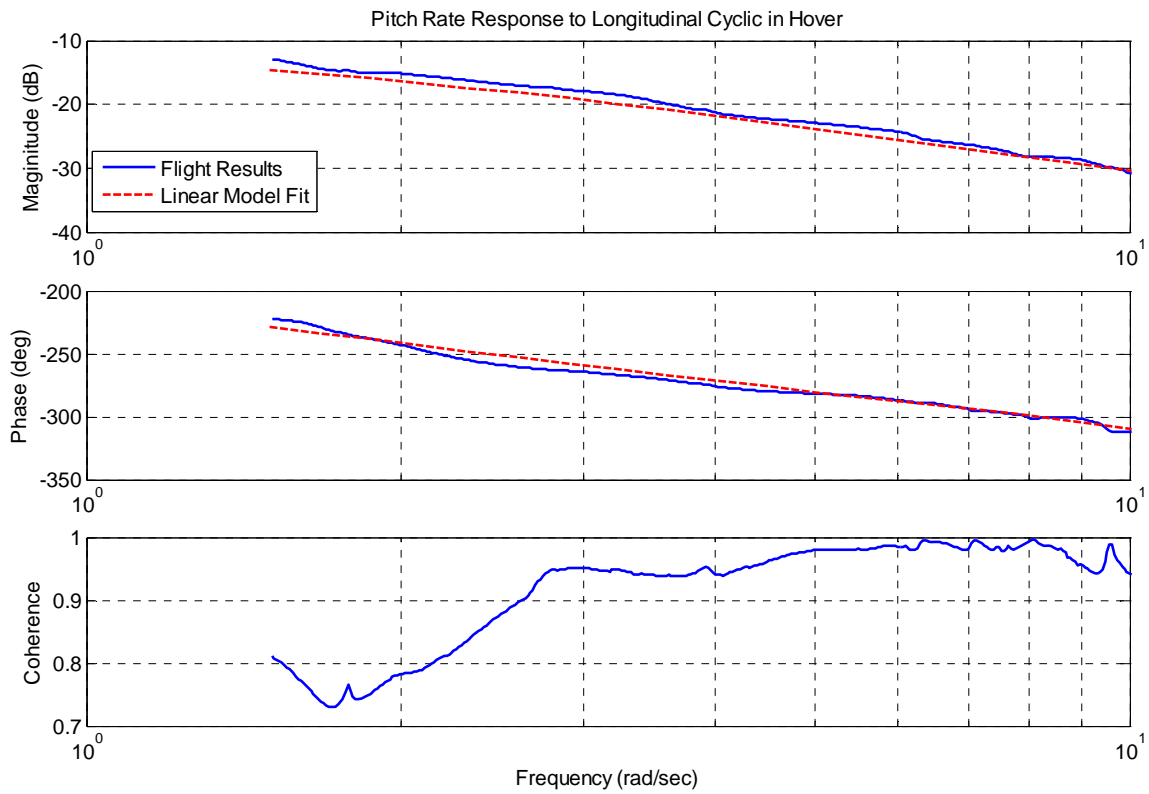


Figure 14. Linear model as compared to flight data for ARH at hover (reprinted from Ref. 4).

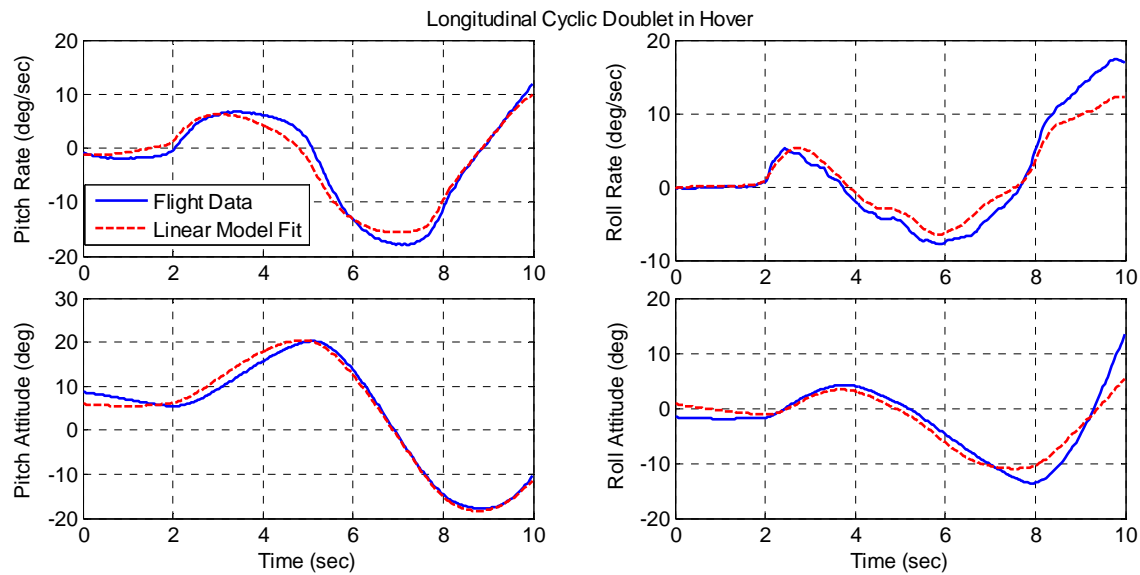


Figure 15. Time Domain Verification for longitudinal axis for ARH at hover (reprinted from Ref. 4).

Validation of the control law block diagrams

Once the model was identified, the next step was to check that the block diagrams were correct by doing frequency response identification of the aircraft with control laws turned on. In an ideal situation, the block diagrams would be validated by doing a broken loop analysis from flight data and comparing to the block diagram. However, the required data to calculate a broken loop response were not available, so a validation of only the control law portion of the block diagram was performed. This ensures that the control laws are implemented correctly on the aircraft, which is an important part of ensuring that the control laws perform as expected. Considering that the model portion of the block diagram was already validated in the system identification, and that the linkages and actuators were well known, checking only the control law portion of the block diagram was a reasonable compromise.

In order to identify the control laws on the aircraft, the feedback was isolated by conducting an electronic frequency sweep via the SCAS actuator, while the pilot stayed off the controls as much as possible. The input to the frequency response calculation was the feedback signal as measured on the aircraft (pilot input = 0) and the output was the SCAS actuator command, as indicated by Fig. 16. The modeled control law frequency responses were also generated with the same input data as from the aircraft, but the output was from the block diagram. This was important because there are nonlinearities in the control systems that are dependent on amplitude. By using the same input signals, this ensures that both the aircraft flight control system and the block diagram treat nonlinearities in the same way and as such, the final frequency responses will match if the block diagram is accurate.

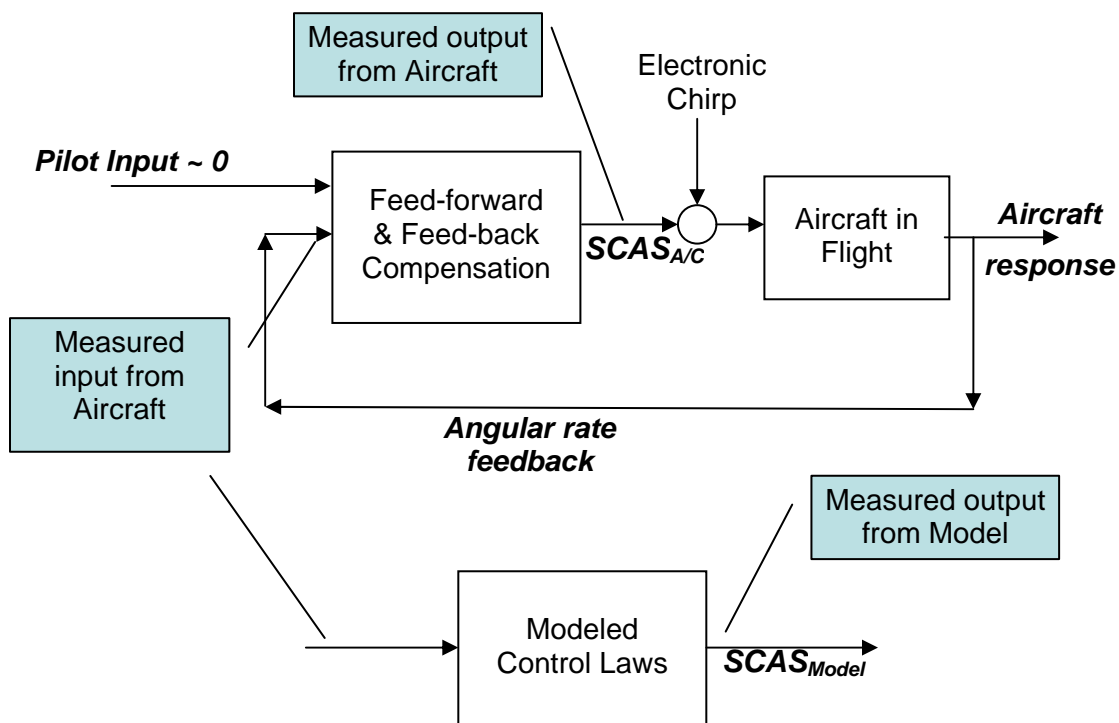


Figure 16. Control law model validation schematic.

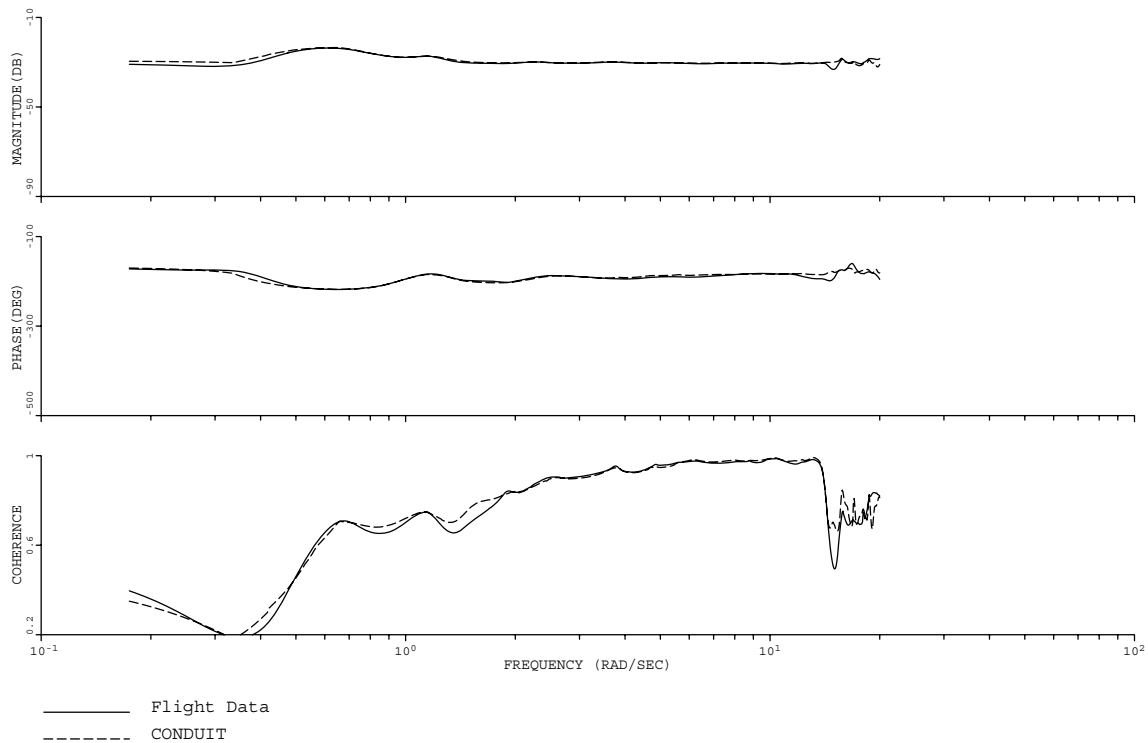


Figure 17. Validation of flight control block diagrams for ARH

An example of a typical validation is shown in Fig. 17. As shown, the model matches the aircraft data, indicating that the block diagram control laws are the same as those implemented on the aircraft. This shows that even though there were nonlinearities in the control laws, frequency domain methods can be accurately used to provide important validation data.

Once the control laws were validated, the engineers were able to move forward with the control law optimization process. The control law optimization is described in Ref. 4.

Lessons Learned on ARH

According to the engineers on the program, the system identification process provided a large time savings. In fact, the lead handling qualities engineer on the program wrote in the conclusions of Ref. 4, “The ARH-70A flight control development effort stands out as an excellent example of how linear modeling, gain optimization and simulation can deliver the best possible flight control design with a minimal amount of flight testing required for design validation.” System identification made this possible by providing a fast and accurate method for modeling the dynamics and validating the control laws.

Future Challenges

System identification methods were very useful in resolving flight control challenges for the rotorcraft case studies presented in the previous sections. These rotorcraft however, are examples of upgrades or civilian aircraft that are being converted to military use. Thus, these aircraft are well known configurations that have been flying in some capacity for many years, and as such few real surprises in the dynamics arose during the system identification. Additionally, these aircraft are of average size and gross weight, for which the modeling, flight control, and handling qualities requirements and challenges are well known. Future configurations include the extremes of very large and very small aircraft, whose dynamics and handling qualities are not well known. The Joint Heavy Lift (JHL) program represents the extreme of a very large rotorcraft. On the other extreme, many small UAVs are being developed for use in military and civilian applications. System

identification from flight data could be used to help meet flight control requirements for these new configurations.

Joint Heavy Lift

The main challenge expected for the JHL is the presence of structural modes in the frequency range of interest for flight control due to the flexible nature of large aircraft. The ability to accurately model these structural modes will clearly be important for flight control design.

Parametric Modeling of Structural Modes

Structural mode modeling has been successfully performed using system identification for a large transport aircraft (Ref. 12). The simple model structure used for that aircraft included a second order system to represent the structural dynamics. The structural dynamics were added to the equations of motion as shown for the lateral dynamics:

$$\dot{p} = L_{\beta}\beta + L_p p + L_r r + L_{\delta_{ail}}\delta_{ail} + L_{\delta_{flp}}\delta_{flp} + L_{\delta_{rud}}\delta_{rud} + \Phi_{p1}\dot{\eta}_{11} \quad (29)$$

where the structural dynamics take the simple modal form:

$$\dot{\eta}_{11} = \eta_{12} \quad (30)$$

$$\begin{aligned} \dot{\eta}_{12} = & -\omega^2\eta_{11} - 2\zeta\omega\eta_{12} + \mu_{wb-p}p \\ & + \mu_{wb-ail}\delta_{ail} + \mu_{wb-flp}\delta_{flp} \end{aligned} \quad (31)$$

A conclusion of this work was that this model structure can be used to represent the structural dynamics. As an example, the identification of the lateral fuselage bending mode is shown as compared to flight data in Fig. 18. The study in Ref. 12 indicated that these methods are accurate and time-efficient for determining a model that contains structural modes for the purpose of flight control analysis. Similar methods could be used to model structural modes for Joint Heavy Lift.

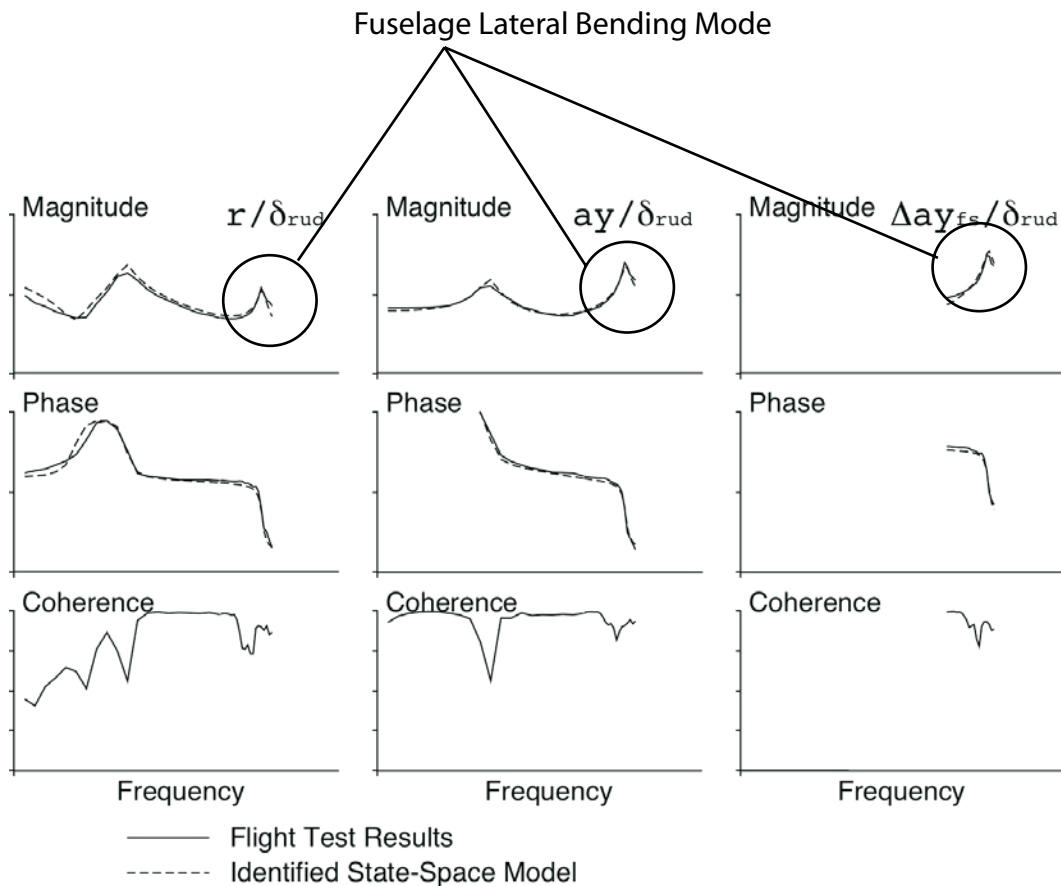


Figure 18. Comparison of model and flight data for lateral dynamics for a large transport aircraft (reprinted from Ref. 12).

Non-parametric Modeling of Structural Modes

Parametric modeling of all the structural and rotor-modes can be very time consuming due to the coupled and overlapping nature of these modes. A non-parametric analysis method can be used to replace the state-space model with a frequency response from flight data, which will contain the un-modeled modes (as long as it has good coherence at those modes), to generate a broken-loop response. Then stability margins can be accurately evaluated over the frequency range of the un-modeled modes. This could be used on the JHL to easily determine stability margins with respect to structural modes that are not included or accurately represented in the state-space model.

In the analysis, the block diagram should be setup similarly to that shown in Fig. 19. The broken loop is calculated by multiplying the flight identified frequency response with the control system frequency response. The state-space model is still in place for all off-axis inputs, and a single frequency response replaces the

dynamics for the on-axis input/output response. This method ignores the effect of off-axis couplings on the calculated on-axis broken loop response, but these have a small effect when the off-axis loops are closed. This will produce an accurate broken loop response, which can then be used to determine stability margins in the frequency range of the un-modeled modes.

This was performed on the UH-60M to predict stability margins associated with the progressive lag mode around 34 rad/s, which was not accurately determined by the state-space model (Ref. 6). For the baseline gains, a low gain margin associated with this mode was not predicted by the state-space model as shown in Fig. 20. By using the actual frequency response from flight in place of the state-space model, the low gain margin that was observed in flight by an oscillation could be predicted in the analysis. Using this same method, new gains were optimized that did not destabilize the progressive lag mode.

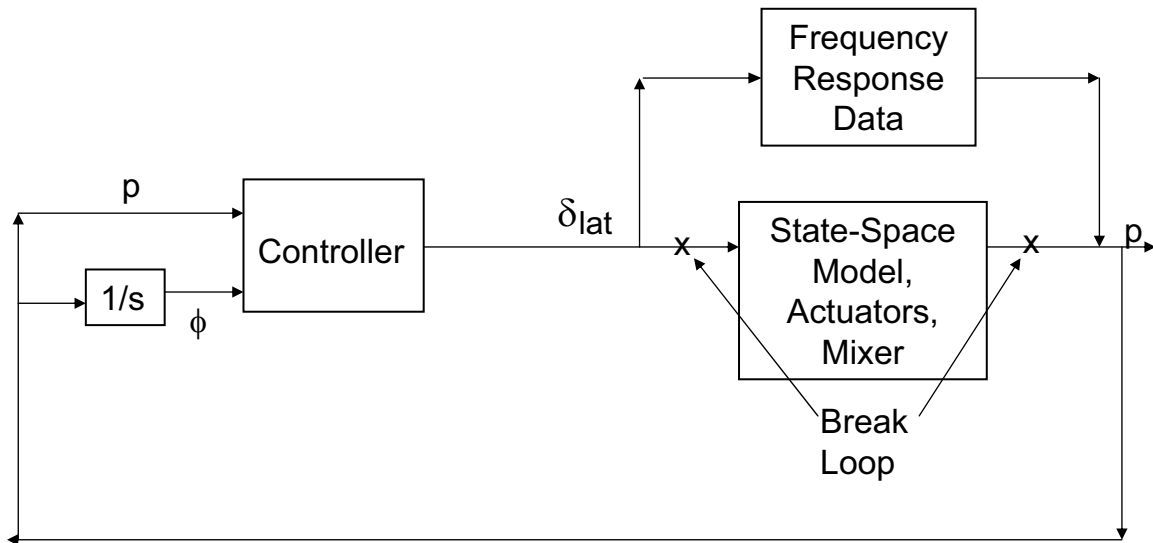


Figure 19. Block Diagram showing use of non-parametric model in flight control analysis.

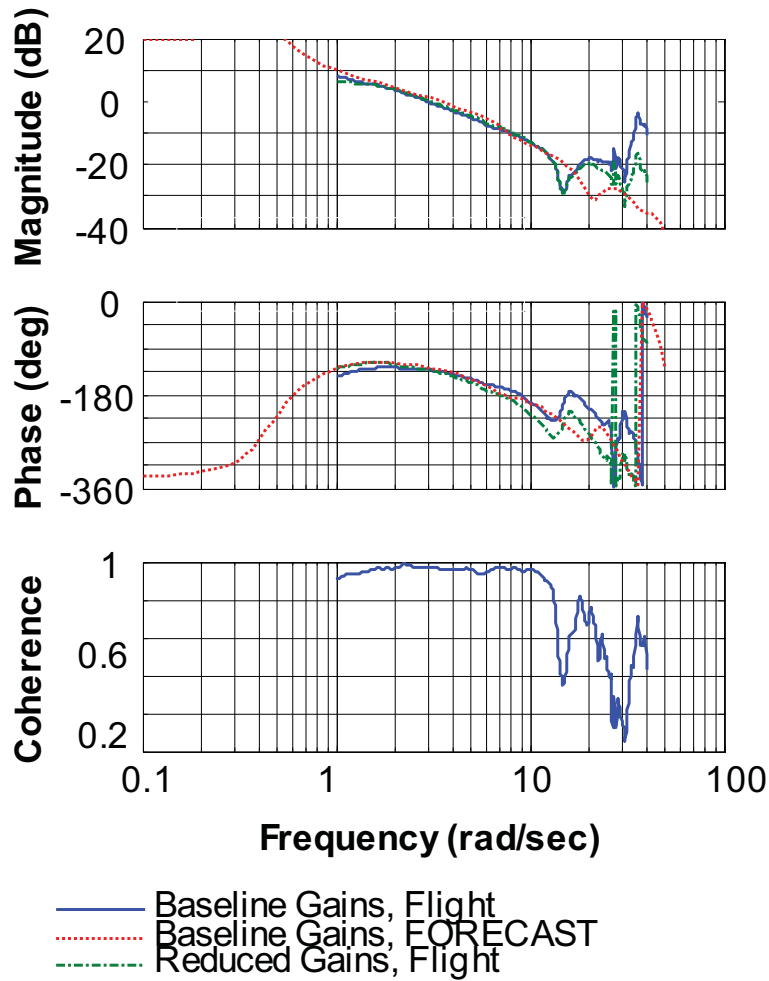


Figure 20. Pitch stability from analysis of flight test measured response (reprinted from Ref. 6).

An uncertainty analysis of the non-parametric model can also be included in these broken loop calculations. This is especially important in cases like Fig. 20 because of low coherence, indicating low accuracy, around some of the modes of interest. For an identified frequency response, the uncertainty is characterized with the random error function. The random error is a function of the coherence and the number of averages used in the computation of a frequency response (Ref. 2):

$$\varepsilon_r = C_\varepsilon \frac{[1 - \gamma_{xy}^2]^{0.5}}{|\gamma_{xy}| \sqrt{2n_d}} \quad (32)$$

where C_ε is a constant to account for the 80% window overlap, γ_{xy}^2 is the coherence function, and n_d is the number of independent time history averages (T_{record}/T_{window}).

From the equation above, it can be seen that high coherence and a high number of averages produces a small random error function. The random error can be related to the 95% confidence limits on the magnitude and phase curves. For small normalized random error (ε_r), random error is approximately equal to the standard deviation (Ref. 13). This indicates that the confidence intervals are given by:

For magnitude:

$$\hat{H}(1 - 2\varepsilon_r) \leq |H| \leq \hat{H}(1 + 2\varepsilon_r) \quad (33)$$

with 95% confidence, where $|H|$ is the true magnitude and \hat{H} is the estimated magnitude

For phase:

$$\hat{\phi} - 2\varepsilon_r \leq \phi \leq \hat{\phi} + 2\varepsilon_r \text{ (in rad)} \quad (34)$$

with 95% confidence, where $|\phi|$ is the true phase and $\hat{\phi}$ is the estimated phase

Then, referring to Fig. 19, the state-space model for p/δ_{lat} would be replaced with the flight identified frequency response data for p/δ_{lat} with +/- 95% confidence intervals included.

As an example of the analysis, the results of a non-parametric uncertainty analysis of an example XV-15 case are shown. The random error bounds (95% confidence limits) were then applied to the identified frequency response, and the gain and phase margins determined as shown in Fig. 21.

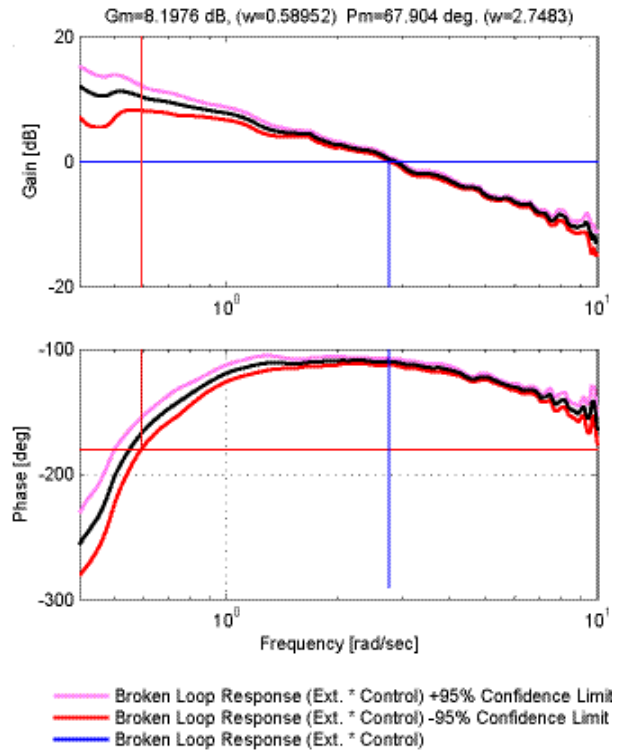


Figure 21. Lateral broken loop frequency responses with uncertainty for MQ-8B at hover.

For the worst case, which is the combination of the lower magnitude and lower phase bound, the low frequency gain margin decreases from 13.85 dB to 8.19 dB. This case still meets the requirement of 6 dB gain margin since extra margin was built in. The phase margin changes no more than a few degrees for any combination, because of the good coherence around cross-over. The confidence intervals have a small effect in this case because the coherence functions are good over the frequency range of interest. However, if the frequency response models had low coherence as is often the case at lightly damped structural or rotor modes, the uncertainty analysis would have a more drastic result. For the JHL configuration, similar methods could be used to determine the effect of non-parametric uncertainty on stability margins around structural and rotor modes that are not parametrically modeled.

Unmanned Aerial Vehicles

Small unmanned aerial vehicles are being developed for civilian and military surveillance purposes. Unmanned aerial vehicles are often unique configurations so their dynamics are not well known. Additionally, UAVs are also often on rapid development schedules, leaving insufficient time to develop a full physics based non-linear model. System identification can quickly provide both dynamic frequency response information and

parametric models. Rapid system identification has been very useful for UAV applications in the past (Ref. 14). As example of this was rapid system identification of an R-50 helicopter in Ref. 14, which used coupled rotor-fuselage dynamics (similar to S-76) to achieve a good match in the roll rate response. A comparison between the R-50 flight data and the model is given in the paper, and is shown in Fig. 22. The results indicate that these higher-order modeling methods for large rotorcraft also work well on small rotorcraft, and provide a wide frequency range of accuracy.

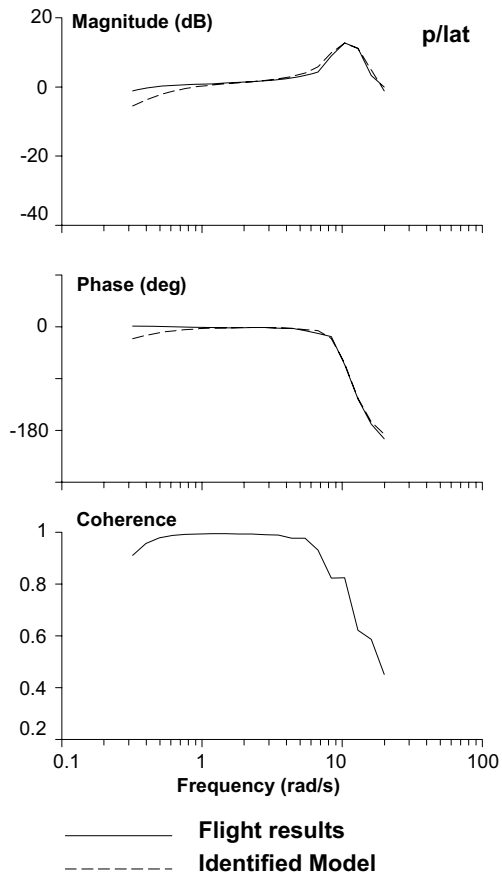


Figure 22. R-50 model and flight data comparison (reprinted from Ref. 14).

Further examples include the use of system identification methods on the 3 meter rotor diameter RMAX (Ref. 15), and the 50.5 cm rotor diameter E-sky electric helicopter (Ref. 16). Both references conclude that system identification is an effective method for identification of small unmanned aerial vehicles.

Conclusions

This paper has shown how system identification can be used to meet flight control development requirements by giving case studies for rotorcraft programs that have recently utilized this modeling method. The case studies show that system identification can efficiently provide:

1. Models with both function and physical fidelity.
2. Precise control over the frequency range of accuracy through choice of model structure.
3. The ability to integrate uncertainty analysis directly from the model to flight control analysis.
4. A method for validating the flight control block diagram, even in the presence of nonlinearities.

These capabilities will be important for new rotorcraft configurations including large flexible vehicles, and small unique unmanned configurations. System identification techniques provided solutions to complex flight control and modeling challenges on recent rotorcraft applications, and will also be able to do so for upcoming flight control design efforts.

References

1. Tischler, M.B., et al, "A Multidisciplinary Flight Control Development Environment and Its Application to a Helicopter," IEEE Control Systems Magazine, Vol. 19, No. 4, pg 22-33, August, 1999.
2. Tischler, M.B, Remple, R.K., Aircraft and Rotorcraft System Identification: Engineering Methods with Flight Test Examples, AIAA Aug 2006.
3. Irwin, J.G., Blanken C. L., Einthoven, P.G., Miller, D.G., "ADS-33E Predicted and Assigned Low-Speed Handling Qualities of the CH-47F with Digital AFCS," Proceedings of the American Helicopter Society 63rd Annual Forum, May 1-3 2007, Virginia Beach, Virginia.
4. Christensen, K.T., Campbell K.G., Griffith, C.D., Ivler, C.M., Tischler, M.B., Harding, J.W., "Flight Control Development for the ARH-70 Armed Reconnaissance Helicopter Program," Proceedings of the American Helicopter Society 63rd Annual Forum, May 1-3 2007, Virginia Beach, Virginia.
5. Quiding, C., Ivler, C.M., Tischler, M.B., "GenHel S-76C Model Correlation using Flight Test Identified Models," Proceedings of the American Helicopter Society 64th Annual Forum, April 29th – May 1st 2008, Montreal, Canada.
6. Fletcher et al, "UH-60M Upgrade Fly-By-Wire Flight Control Risk Reduction using the RASCAL JUH-60 In Flight Simulator," American Helicopter

- Society 64th Annual Forum, April 29th – May 1st 2008, Montreal, Canada
7. Downs, J., Prentice, R., Dalzell, S., Besachio, A., Ivler, C.M., Tischler, M.B., Mansur, M.H., “Control System Development and Flight Test Experience with the MQ-8B Fire Scout Vertical Take-Off Unmanned Aerial Vehicle (VTUAV),” Proceedings of the American Helicopter Society 63rd Annual Forum, May 1-3 2007, Virginia Beach, Virginia.
 8. “Flight Control Design – Best Practices,” NATO-TRO-029, December 2000.
 9. Padfield, Gareth, D., Helicopter Flight Dynamics: The Theory and Application of Flying Qualities and Simulation, AIAA 1996.
 10. Tischler, M.B., “System Identification Requirements for High-Bandwidth Rotorcraft Flight Control System Design,” Journal of Guidance, Control and Dynamics, Volume 13, Number 5, Sep-Oct 1990, Pages 835-841.
 11. Anon, “AS94900 Aerospace- Flight Control System –Design, Installation and Test of Piloted Military Aircraft, General Specification For”, SAE Aerospace 2007.
 12. Theodore, C., Ivler, C., Tischler, M.B., Field, E., Neville, R., Ross, H, “System Identification of a Large Flexible Transport Aircraft”, AIAA Atmospheric Flight Mechanics Conference and Exhibit, August 18th- 21st 2008, Honolulu, Hawaii
 13. Bendat, J.S., Peirsol A.G., Random Data, 2nd Edition, John Wiley & Sons Inc., 1986..
 14. Theodore, C.R., Tischler, M.B., Colbourne, J.D., “Rapid Frequency Domain Modeling Methods for UAV Flight Control Applications,” AIAA Atmospheric Flight Mechanics Conference and Exhibit, August 11-14th 2003, Austin, Texas.
 15. Cheng, R.P., Tischler, M.B., Schulein, G. J., “R-MAX Helicopter State-Space Model Identification for Hover and Forward-Flight”, Journal of the American Helicopter Society, Vol. 51, no. 2, pp. 202, April 2006.
 16. Conroy, J., Pines, D., “System Identification of a Miniature Electric Helicopter using MEMS Inertial, Optic Flow, and Sonar Sensing,” Proceedings of the American Helicopter Society 63rd Annual Forum, May 1-3 2007, Virginia Beach, VA.